Supplement of The Cryosphere, 12, 1415–1431, 2018
https://doi.org/10.5194/tc-12-1415-2018-supplement

The Cryosphere Open Access EGU

Supplement of

Changes in flow of Crosson and Dotson ice shelves, West Antarctica, in response to elevated melt

David A. Lilien et al.

Correspondence to: David A. Lilien (dal22@uw.edu)

1 Evidence against marine ice accretion on Dotson

Significant marine ice accretion downstream of the transverse portion of the channel on Dotson should cause a discrepancy between measurements of freeboard and ice thickness. Ice penetrating radar generally does not penetrate into saline marine ice (Crabtree and Doake, 1986; Robin et al., 1983; Thyssen, 1988), so the bottom reflector from the MCoRDS radar comes from the fresh/saline transition in areas with accreted ice. The radar measurement thus indicates the thickness of fresh ice only, while the freeboard is determined by the total ice thickness, including marine ice. In areas of marine ice, the difference between the full thickness and the fresh ice thickness should cause the actual freeboard to be greater than that which would be calculated from the thickness of the fresh ice alone.

To determine whether there is marine ice accretion on Dotson, we calculate an expected freeboard from ice-thickness measurements made by the MCorDS radar and compare this expected freeboard to surface elevations measured simultaneously by the ATM. To calculate freeboard from the MCorDS radar product, two firn corrections must be made: (1) radar waves propagate at different speeds in ice and firn, which is not accounted for in the estimates of thickness from the MCorDS radar and (2) the total thickness of the shelf includes the air in the firn, so the freeboard is greater would be expected if the full column were the density of ice. To correct for the propagation speed difference, we calculate the 2-way travel from the MCorDS thickness, then convert that value back to depth using a propagation speed that accounts for firn-air content. We calculate a floatation height from this thickness by assuming the column is pure ice, then add to that the thickness of the air column to obtain the final estimate for expected freeboard. For both of these calculations, we assume a constant firn-air content of 13 m. This value is near the median of the spatially variable values we calculate in the main text, and using a spatially constant value prevents aliasing marine ice as variations in firn-air content. We compare surface elevations calculated using hydrostatic equilibrium to the surface elevations from the ATM, which we reference to the EGM2008 geoid and interpolate onto the MCoRDS data using the 5 nearest points, slope correcting and weighting by inverse square distance.

Along flight lines approximately parallel to flow, we find that the freeboard height calculated from ice thickness corresponds to measured surface elevation with standard deviations ranging from 2.9-4.3 m. The channel has a surface expression of 10 m over large portions of these flightlines and up to 15 m in places, so the channel is deep compared to the errors in our method. We the calculated freeboard to have 3-4 m bias towards a higher surface than the direct freeboard measurements, opposite of what is expected if marine ice is present. Further, we find no correlation between distance along flow and misfit between observed and measured ice thickness. If marine ice accreted downstream of this channel, we would expect a trend towards the hydrostatic calculation of freeboard being smaller than the freeboard measured with the ATM farther downstream. Thus, we conclude that the thickening downstream of the channel on Dotson is not caused by marine ice accretion, but rather by dynamic thinning or a temporal change in melt.

2 Calculation of melt rates following Khazendar et al. (2016)

We converted the thinning rates in Khazendar et al. (2016), which represent anomalous thinning under the assumption of no dynamic thinning, to melt rates using the flux divergence. As in Khazendar et al., we first calculated the thinning rate at each crossover of the MCorDS radar over Crosson and Dotson, and our values for the thinning rate agree to within error for the 27 points that they do not identify as anomalous (Table S2). To obtain the flux divergence correction, we resampled velocity and ice thickness to a 1000-m grid and calculated the flux divergence at each grid point. We then linearly interpolated the flux divergence from the grid to each radar crossover and subtracted this value from the thinning rate to obtain the melt rate. We plot the melt rate in Figure S1 and present the values in Table S1. The peak value we find (187 m a^{-1}) is greater than the peak thinning rate found in Khazendar et al. (2016), though the magnitude of melt that we find is generally comparable to the thinning rates in the area. The distribution of melt is different than the distribution of thinning found in Khazendar et al. (2016), but as expected melt is highest near the grounding line and decreases downstream. These recalculated values are still sensitive to advection of heterogeneous properties of the shelf (e.g. crevasses or parcels of thick ice) that are not accounted for in the flux divergence, and thus may not be representative of melt.

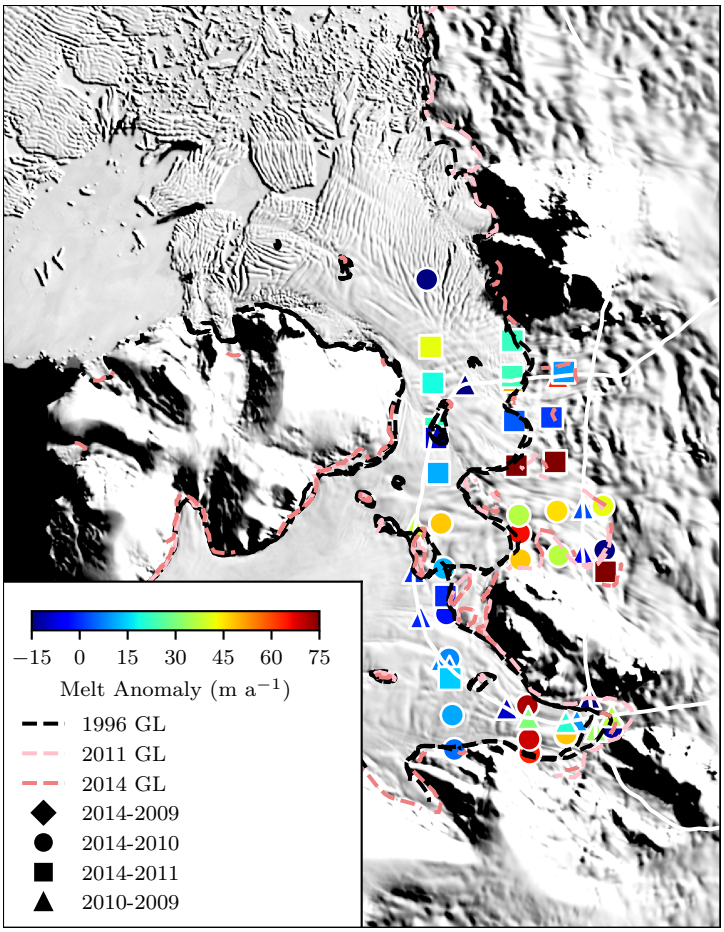

3

Figure S1. Melt rate anomalies, calculated using the thinning rate and flux divergence, at crossover points of Operation Icebridge flightlines 2009-2014. Color indicates melt rate, and shape of the symbol indicates the years of crossover. Dashed lines show grounding lines, and the solid white line indicates the flightpath repeated in 2002 and 2009. See Khazendar et al. (2016).

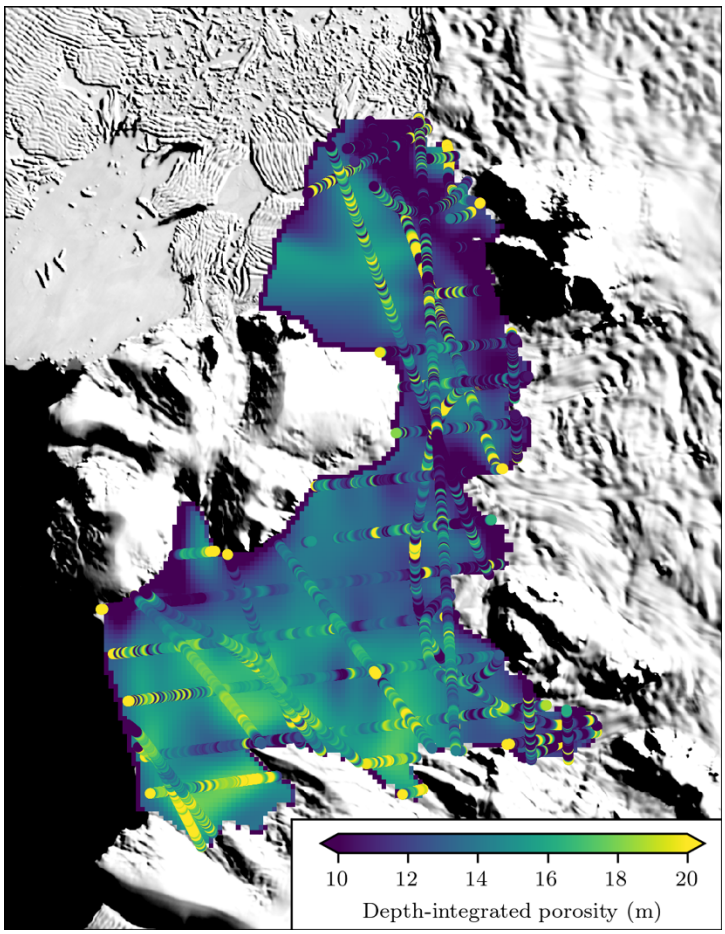

Figure S2. Depth-integrated porosity (firn-air content) over Crosson and Dotson ice shelves. Colors in the background show gridded product, colored circles show individual radar traces from the MCoRDS radar.

Point Number	$\partial H/\partial t$(m a^{-1})	$\partial H/\partial t$ (m a^{-1}) from (Khazendar et al., 2016)	Anomalous melt rate (m a^{-1})
1	-2	-3	23
2	-10	-10	10
3	49	38	63
4	27	30	50
5	2	5	1
6	51	44	106
7	139	129	127
8	24	16	42
9	20	14	46
10	0	-2	36
11	43	37	66
12	59	51	48
13	36	18	37
14	66	57	-30
15	41	44	3
16	59	65	-7
17	88	83	187
18	37	32	72
19	22	13	69
20	35	33	64
21	21	19	48
22	15	15	37
23	-13	-20	-13
24	-15	109	34
25	-18	-9	10
26	22	19	37
27	10	13	21
28	18	19	30

Table S1. Comparison of values for thinning and melt rate here and in Khazendar et al. (2016). We retain the numbering of points used in that paper's supplementary material. Columns 2 and 3 show the thickness changes estimated here and that paper respectively. Column 4 shows the melt rate, calculated by subtracting the flux divergence from the thinning rate. Note that Khazendar et al. identify point 24 as anomalous, though the value we calculate is similar to others in the area.